

# Orbital Pumping by Magnetization Dynamics in Ferromagnets

Dongwook Go,<sup>1,2,\*</sup> Kazuya Ando,<sup>3,4,5</sup> Armando Pezo,<sup>6</sup> Stefan Blügel,<sup>1</sup> Aurélien Manchon,<sup>6</sup> and Yuriy Mokrousov<sup>1,2</sup>

<sup>1</sup>*Peter Grünberg Institut and Institute for Advanced Simulation, Forschungszentrum Jülich and JARA, 52425 Jülich, Germany*

<sup>2</sup>*Institute of Physics, Johannes Gutenberg University Mainz, 55099 Mainz, Germany*

<sup>3</sup>*Department of Applied Physics and Physico-Informatics, Keio University, Yokohama 223-8522, Japan*

<sup>4</sup>*Keio Institute of Pure and Applied Sciences (KiPAS), Keio University, Yokohama 223-8522, Japan*

<sup>5</sup>*Center for Spintronics Research Network (CSRN), Keio University, Yokohama 223-8522, Japan*

<sup>6</sup>*Aix-Marseille Université, CNRS, CINaM, Marseille, France*

(Dated: September 27, 2023)

We show that dynamics of the magnetization in ferromagnets can pump the orbital angular momentum, which we denote by orbital pumping. This is the reciprocal phenomenon to the orbital torque that induces magnetization dynamics by the orbital angular momentum in non-equilibrium. The orbital pumping is analogous to the spin pumping established in spintronics but requires the spin-orbit coupling for the orbital angular momentum to interact with the magnetization. We develop a formalism that describes the generation of the orbital angular momentum by magnetization dynamics within the adiabatic perturbation theory. Based on this, we perform first-principles calculation of the orbital pumping in prototypical 3d ferromagnets, Fe, Co, and Ni. The results show that the ratio between the orbital pumping and the spin pumping ranges from 5 to 15 percents, being smallest in Fe and largest in Ni. This implies that ferromagnetic Ni is a good candidate for measuring the orbital pumping. Implications of our results on experiments are also discussed.

Injection of spin into a ferromagnet can induce magnetization dynamics, which is called the spin torque [1–5]. The reciprocal effect to the spin torque is known as the spin pumping, which refers to generation of non-equilibrium spin by magnetization dynamics [6–10]. The spin torque and spin pumping have played pivotal roles in the development of spintronics as means of manipulating the magnetization and generating spin currents, respectively [11, 12]. In general, however, the physical mechanism of magnetization dynamics is governed by transfer of the *angular momentum* [13, 14], which is not restricted to the spin. Thus, magnetization dynamics can also be driven by the orbital angular momentum (OAM) induced out of equilibrium [15]. This so-called orbital torque can be regarded as an orbital analog of the spin torque. A crucial difference between the spin torque and the orbital torque is that the orbital torque requires the spin-orbit coupling (SOC). This is because local moments in a ferromagnet are coupled to spin by the exchange interaction, and the OAM interacts with magnetization *indirectly* via SOC. Thus, the orbital torque depends sensitively on the way the spin and orbital characters are entangled in the wave functions of the states near the Fermi energy [14, 16]. The orbital torque has been measured in several experiments in recent years, via the sign change, crucial dependence on the choice of a ferromagnet, and orbital-to-spin conversion [16–24].

A natural question that arises is what are the properties of the reciprocal phenomenon to the orbital torque. We denote this by *orbital pumping*, generation of non-equilibrium OAM from dynamics of the magnetization, whose concept is schematically illustrated in Fig. 1. Recently, Hayashi *et al.* reported an experimental observation of the orbital pumping in Ti/Ni bilayers [25]. Here, the ferromagnetic resonance generates the OAM together with the spin in Ni, which is injected across the interface. The injected OAM in Ti is electrically measured by using the inverse orbital Hall effect, where

the inverse spin Hall effect is negligibly small due to small SOC [26, 27]. This result is consistent with the recent observation of large orbital Hall effect in Ti [27] and the orbital torque measurement which finds pronounced torque response when Ni is used as a ferromagnet [23]. Interestingly, Hayashi *et al.* found that the signal is significantly suppressed in Ti/Fe bilayers [25], implying that the orbital pumping is less pronounced in Fe. One may ask what makes the difference of the orbital pumping between Fe and Ni. This motivates us to investigate its microscopic origin and perform quantitative evaluation of the orbital pumping in 3d ferromagnets.

In this Letter, we develop a formalism describing the orbital pumping within the adiabatic perturbation theory and derive a Green’s function expression for the generation of the OAM by magnetization dynamics. By first-principles methods, we compute the orbital pumping in ferromagnetic Fe, Co, and Ni. We show that the orbital pumping is a concomitant effect of the spin pumping due to the SOC and thus exhibits a Hund-rule-like behavior [28, 29], evolving from the negative to the positive value as the occupation number of the *d* shell increases. The magnitude of the orbital pumping ranges from

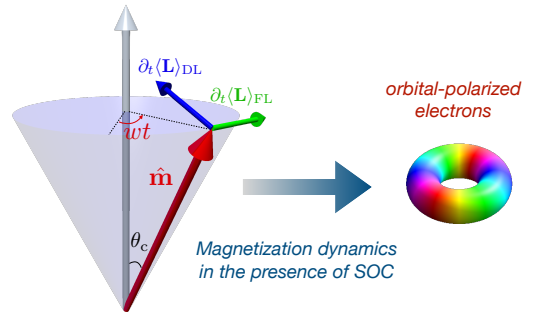


FIG. 1. Concept of the orbital pumping.

5 to 15 percents of that of the spin pumping in Fe, Co, and Ni, being is smallest in Fe and largest in Ni. This result explains the recent experiment measuring significant orbital pumping contribution in Ti/Ni [25], but we find that the almost complete suppression in Ti/Fe cannot be explained by the bulk property of Fe alone.

We define the orbital pumping as the response of  $\partial_t \langle \mathbf{L} \rangle$  to the magnetization dynamics, where  $\mathbf{L}$  is the OAM operator. This can be formally written as a linear response expression,

$$\partial_t \langle L_\alpha \rangle = \sum_{\beta} \chi_{\alpha\beta}^L (\hat{\mathbf{m}} \times \partial_t \hat{\mathbf{m}})_\beta, \quad (1)$$

where  $\hat{\mathbf{m}}$  is the unit vector of the magnetization, and  $\alpha, \beta$  are Cartesian indices. Note that  $\hat{\mathbf{m}} \times \partial_t \hat{\mathbf{m}}$  acts as a generalized force, and points in the direction of the Gilbert damping. As shown in Fig. 1,  $\partial_t \langle \mathbf{L} \rangle$  can be conveniently decomposed into fieldlike and dampinglike components, which point in the directions of  $\partial_t \hat{\mathbf{m}}$  and  $\hat{\mathbf{m}} \times \partial_t \hat{\mathbf{m}}$ , respectively. Let us consider a situation of the magnetization precessing around a certain axis (grey arrow) with the cone angle  $\theta_c$  and angular frequency  $w$ . For convenience, let us define Cartesian coordinates such that  $x$ ,  $y$ , and  $z$  are axes parallel to  $\partial_t \hat{\mathbf{m}}$ ,  $\hat{\mathbf{m}} \times \partial_t \hat{\mathbf{m}}$ , and  $\hat{\mathbf{m}}$ , respectively. From Eq. (1), we find  $\partial \langle \mathbf{L} \rangle_{\text{FL}} = \hat{\mathbf{x}} \chi_{xx}^L w \sin \theta_c$  and  $\partial \langle \mathbf{L} \rangle_{\text{DL}} = \hat{\mathbf{y}} \chi_{yy}^L w \sin \theta_c$ , where  $w \sin \theta_c$  is the norm of  $\hat{\mathbf{m}} \times \partial_t \hat{\mathbf{m}}$ . Both the fieldlike and dampinglike components have AC responses, but the projection of the dampinglike component on the precession axis generates a DC response, which is given by  $\chi_{yy}^L w \sin^2 \theta_c$ .

To evaluate  $\chi_{\alpha\beta}^L$  from the electronic structure, we apply the adiabatic perturbation theory [30], in which  $\hat{\mathbf{m}}$  evolves slowly enough for the electronic eigenstates to evolve adiabatically. From this, we derive a Green's function's expression for  $\chi_{\alpha\beta}^L$  [31] in the Bastin-Smrčka-Středa's form [32–34] of the Kubo formula [35],

$$\chi_{\alpha\beta,\text{even}}^L = \frac{\hbar}{4\pi} \int d\mathcal{E} (\partial_{\mathcal{E}} f) \quad (2a)$$

$$\times \text{Tr} \left[ T_{\text{tot}}^{L\alpha} (G^{\text{R}} - G^{\text{A}}) T_{\text{XC}}^{S\beta} (G^{\text{R}} - G^{\text{A}}) \right],$$

$$\chi_{\alpha\beta,\text{odd}}^L = \frac{\hbar}{4\pi} \int d\mathcal{E} f \quad (2b)$$

$$\times \text{Tr} \left[ T_{\text{tot}}^{L\alpha} (G^{\text{R}} - G^{\text{A}}) T_{\text{XC}}^{S\beta} (\partial_{\mathcal{E}} G^{\text{R}} + \partial_{\mathcal{E}} G^{\text{A}}) \right. \\ \left. - T_{\text{tot}}^{L\alpha} (\partial_{\mathcal{E}} G^{\text{R}} + \partial_{\mathcal{E}} G^{\text{A}}) T_{\text{XC}}^{S\beta} (G^{\text{R}} - G^{\text{A}}) \right],$$

where  $G^{\text{R/A}} = 1/(\mathcal{E} - \mathcal{H}_{\text{tot}} \pm i\Gamma)$  is the retarded/advanced Green's function,  $\mathcal{H}_{\text{tot}}$  is the total Hamiltonian,  $\mathcal{E}$  is the energy, and  $\Gamma$  is energy broadening, which effectively describes relaxation of the electron quasiparticles by scatterings. The Fermi-Dirac distribution function  $f$  is defined at energy  $\mathcal{E}$ . The operators  $T_{\text{tot}}^{L\alpha} = [L_\alpha, \mathcal{H}_{\text{tot}}]/i\hbar$  and  $T_{\text{XC}}^{S\beta} = [S_\beta, \mathcal{H}_{\text{XC}}]/i\hbar = J(\mathbf{r})\hat{\mathbf{m}} \times \mathbf{S}$  are the total torque on the  $\alpha$  component of the OAM and the exchange torque on the  $\beta$  component of the spin, respectively. Here,  $\mathcal{H}_{\text{XC}} = J(\mathbf{r}) \hat{\mathbf{m}} \cdot \mathbf{S}$  is the exchange potential.

In Eq. (2), we adopt the decomposition depending on the time-reversal parity of the response [36]. Meanwhile, the analogous expression of Eq. (1) for the spin pumping can be obtained by replacing  $L_\alpha$  by  $S_\alpha$  in Eq. (2). We note that the linear response approach to the spin pumping was also considered in Refs. [37, 38], but the orbital analog has not been studied, to our best knowledge.

The orbital pumping is reciprocal to the orbital torque, whose linear response expression is given by

$$\langle T_{\text{XC}}^{S\alpha} \rangle = \sum_{\beta} \tilde{\chi}_{\alpha\beta}^L B_\beta^L, \quad (3)$$

where  $\tilde{\chi}_{\alpha\beta}^L$  is the response tensor for the orbital torque. Here,  $B_\beta^L$  is an effective field that couples to the OAM by the interaction  $\mathcal{H}_L = \mathbf{B}_L \cdot \mathbf{L}$ . It effectively describes a situation where non-equilibrium OAM is induced, for example, by orbital Hall effect [39–41] or orbital Edelstein effect [42–44]. Note that both  $\partial_t \langle \mathcal{H}_L \rangle = \partial_t \langle \mathbf{L} \rangle \cdot \mathbf{B}^L$  and  $\partial_t \langle \mathcal{H}_{\text{XC}} \rangle = \langle T_{\text{XC}}^{S\alpha} \rangle \cdot (\hat{\mathbf{m}} \times \partial_t \hat{\mathbf{m}}) = \langle J\mathbf{S} \rangle \cdot \partial_t \hat{\mathbf{m}}$  have the unit of *power*. The expression for  $\tilde{\chi}_{\beta\alpha}^L$  can also be derived similarly to Eq. (2), by which the reciprocal relation

$$\chi_{\alpha\beta}^L = \tilde{\chi}_{\beta\alpha}^L \quad (4)$$

can be explicitly shown [31].

We quantitatively evaluate the spin pumping and orbital pumping in prototypical 3d ferromagnets: bcc Fe, hcp Co, and fcc Ni. We set the magnetization  $\hat{\mathbf{m}} = -\hat{z}$ . Details of the computational method can be found in Ref. [31]. For all Fe, Co, and Ni, only  $\chi_{xx,\text{even}}^L$  and  $\chi_{yy,\text{even}}^L$  are nonzero for the time-reversal-even part [Eq. (2a)], and only  $\chi_{xy,\text{odd}}^L$  and  $\chi_{yx,\text{odd}}^L$  are nonzero for the time-reversal-odd part [Eq. (2b)]. This is because of the  $\mathcal{TM}$  symmetry present in the systems, where  $\mathcal{T}$  is the time-reversal and  $\mathcal{M}$  is the reflection with respect to a mirror plane containing the magnetization [31]. Therefore, we drop “even” and “odd” in the subscript of  $\chi_{\alpha\beta}^L$  and  $\chi_{\alpha\beta}^S$  in the discussion below.

The results for the ratio  $\chi_{xx}^L/\chi_{xx}^S$  and  $\chi_{xy}^L/\chi_{xy}^S$  are summarized in Tab. I. The ratios are between 5 and 15 percents, and the magnitudes are in the order of Fe < Co < Ni. We find that the ratios are nearly the same for the two chosen values

Material	$\chi_{xx}^L/\chi_{xx}^S$ [%]	$\chi_{xy}^L/\chi_{xy}^S$ [%]
Fe (25 meV)	6.08	4.38
Co (25 meV)	9.87	9.62
Ni (25 meV)	11.08	15.10
Fe (100 meV)	7.19	4.39
Co (100 meV)	9.53	9.32
Ni (100 meV)	10.64	14.12

TABLE I. The ratio between the orbital pumping and spin pumping in Fe, Co, and Ni for the diagonal and off-diagonal responses, obtained for 25 meV and 100 meV of the energy broadening.

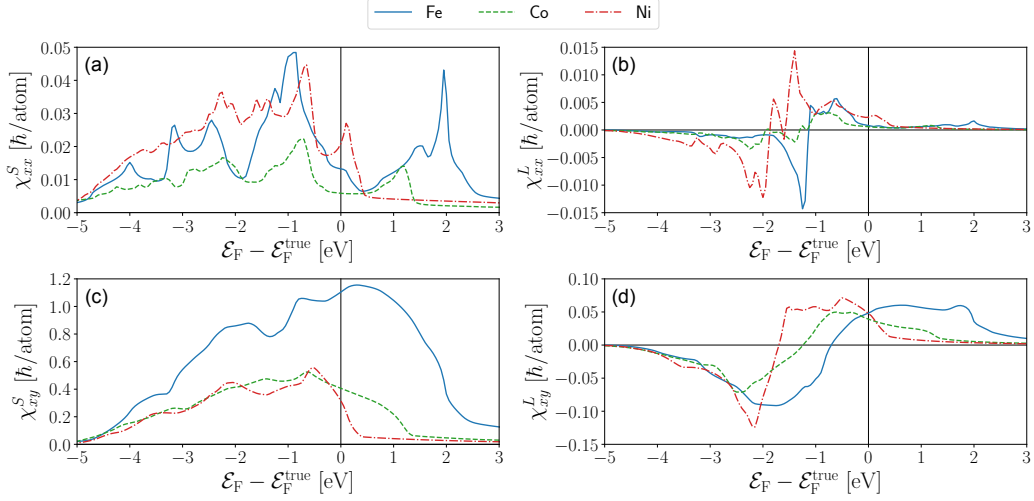


FIG. 2. The plots of the Fermi energy ( $\mathcal{E}_F$ ) dependence of (a)  $\chi_{xx}^S$  and (b)  $\chi_{xx}^L$ , for the spin pumping and orbital pumping, respectively. The same plots for  $\chi_{xy}^S$  and  $\chi_{xy}^L$  are shown in (c) and (d), respectively. The energy broadening is set to  $\Gamma = 25$  meV in evaluating Eq. (2). The Fermi energy is varied with respect to the true value  $\mathcal{E}_F^{\text{true}}$  within the rigid band approximation.

of the energy broadening  $\Gamma$ , 25 meV and 100 meV, implying that the relative magnitude between the orbital pumping and spin pumping is robust with respect to the degree of disorder.

In order to understand what makes Fe, Co, and Ni different, we investigate Fermi energy dependence of both diagonal ( $\chi_{xx}^S$  and  $\chi_{xx}^L$ ) and off-diagonal ( $\chi_{xy}^S$  and  $\chi_{xy}^L$ ) components of the response, which are shown in Figs. 2(a,b) and Figs. 2(c,d), respectively. The sign for the spin pumping [Figs. 2(a,c)] remains positive on a wide range of energy because the spin pumping is mainly due to the exchange spin splitting. The orbital pumping, however, exhibits gradual change of the sign, from negative to positive values [Figs. 2(b,d)]. We find that the orbital pumping is driven by the SOC and vanishes if the SOC is switched off [31]. Therefore, the orbital pumping is a secondary effect that follows the spin pumping by the SOC. This is also why for considered materials the orbital pumping [Figs. 2(b,d)] is generally smaller than the spin pumping [Figs. 2(a,c)] by an order of magnitude.

For transition metals, Hund's third rule [28, 29] states that when the  $d$  shell is approximately less than half-filled, the cor-

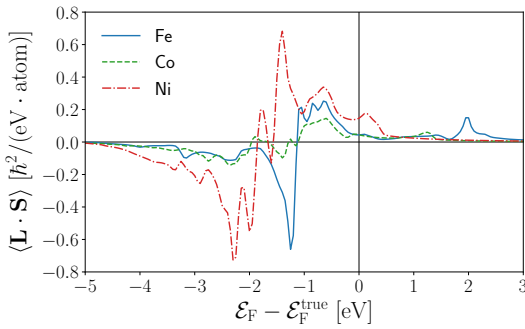


FIG. 3. Correlation between  $\mathbf{L}$  and  $\mathbf{S}$  at the Fermi surface.

relation between  $\mathbf{L}$  and  $\mathbf{S}$  is negative,  $\langle \mathbf{L} \cdot \mathbf{S} \rangle < 0$ , thus the spin pumping and orbital pumping exhibit the opposite signs. When the  $d$  shell is more than half-filled, the correlation becomes positive  $\langle \mathbf{L} \cdot \mathbf{S} \rangle > 0$ , thus the spin pumping and orbital pumping have the same sign. The correlation between  $\mathbf{L}$  and  $\mathbf{S}$  for the states at the Fermi surface is shown in Fig. 3. They all evolve from negative values to positive values as the Fermi energy gradually increases. Note the stark resemblance between Fig. 2(b) and Fig. 3, which clearly demonstrates the crucial role of the correlation between the orbital and spin angular momenta in the orbital pumping.

In general, we find that the diagonal component [Figs. 2(a,b)] exhibits more rapid variation as a function of the energy, as compared to the off-diagonal component [Figs. 2(c,d)]. This is because the  $\mathcal{T}$ -even [Eq. (2a)] and  $\mathcal{T}$ -odd response [Eq. (2b)] capture the contributions at the Fermi surface and from the Fermi sea, respectively. At zero temperature, Eq. (2a) becomes

$$\chi_{\alpha\beta,\text{even}}^L = \frac{\hbar}{\pi} \sum_{\mathbf{k}} \sum_{nm} A_{n\mathbf{k}}(\mathcal{E}_F) A_{m\mathbf{k}}(\mathcal{E}_F) \times \text{Re} \left[ \langle \psi_{n\mathbf{k}} | T_{\text{tot}}^{L\alpha} | \psi_{m\mathbf{k}} \rangle \langle \psi_{m\mathbf{k}} | T_{\text{XC}}^{S\beta} | \psi_{n\mathbf{k}} \rangle \right], \quad (5)$$

where  $\psi_{n\mathbf{k}}$  is the Bloch state with band index  $n$  and crystal momentum  $\mathbf{k}$ , and  $A_{n\mathbf{k}}(\mathcal{E}_F) = \Gamma / [(\mathcal{E}_F - \mathcal{E}_{n\mathbf{k}})^2 + \Gamma^2]$  is the spectral function at the Fermi energy, and  $\mathcal{E}_{n\mathbf{k}}$  is the energy dispersion. On the other hand, the  $\mathcal{T}$ -odd response [Eq. (2b)] has *intrinsic limit* even in the zeroth order of  $\Gamma$ ,

$$\chi_{\alpha\beta,\text{odd}}^L = \hbar \sum_{\mathbf{k}} \sum_{n \neq m} (f_{n\mathbf{k}} - f_{m\mathbf{k}}) \times \frac{\text{Im} \left[ \langle \psi_{n\mathbf{k}} | T_{\text{tot}}^{L\alpha} | \psi_{m\mathbf{k}} \rangle \langle \psi_{m\mathbf{k}} | T_{\text{XC}}^{S\beta} | \psi_{n\mathbf{k}} \rangle \right]}{(\mathcal{E}_{n\mathbf{k}} - \mathcal{E}_{m\mathbf{k}})^2}, \quad (6)$$

where  $f_{n\mathbf{k}}$  is the Fermi-Dirac distribution function.

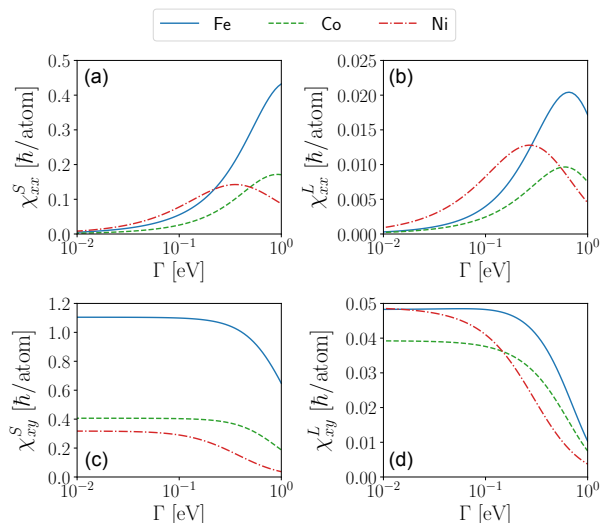


FIG. 4. The plots of the energy broadening ( $\Gamma$ ) dependence of (a)  $\chi_{xx}^S$  and (b)  $\chi_{xx}^L$ , for the spin pumping and orbital pumping, respectively. The same plots for  $\chi_{xy}^S$  and  $\chi_{xy}^L$  are shown in (c) and (d), respectively.

Because of this, the diagonal and off-diagonal responses exhibit different behaviors as a function of the energy broadening  $\Gamma$ . Figures 4(a) and 4(b) show the  $\Gamma$ -dependence of  $\chi_{xx}^S$  and  $\chi_{xx}^L$ , respectively. Interestingly, both of them exhibit non-monotonic behavior. They tend to increase from the ultraclean regime ( $\Gamma \approx 0$ ) to moderately clean regime ( $\Gamma \sim 10^{-1}$  eV), but as  $\Gamma$  further increases toward a disordered regime ( $\Gamma \sim 1$  eV) the magnitudes start to decrease. This suggests that samples need to be moderately clean but not too clean to have sizable magnitude of  $\chi_{xx}^S$  and  $\chi_{xx}^L$ . We emphasize that expressions like Eq. (5) often exhibit a conductivity-like  $\propto 1/\Gamma$  behavior because the band-diagonal term ( $n = m$ ) is proportional to  $A_{n\mathbf{k}}(\mathcal{E}_F)A_{n\mathbf{k}}(\mathcal{E}_F) \approx (\pi/\Gamma)\delta(\mathcal{E}_F - \mathcal{E}_{n\mathbf{k}})$  in small  $\Gamma$  limit [36, 45]. However,  $\chi_{xx}^S$  and  $\chi_{xx}^L$  show a quadratic  $\propto \Gamma^2$  behavior because the band-diagonal component of the torque-torque correlation in Eq. (5) is absent. Therefore, spectral mixing of bands at the Fermi energy is crucial for  $\chi_{xx}^S$  and  $\chi_{xx}^L$ . Meanwhile,  $\chi_{xy}^S$  and  $\chi_{xy}^L$  shown in Figs. 4(c) and 4(d), respectively, are stable up to moderate strength of the broadening, displaying a typical intrinsic behavior.

We generally find that the spin pumping [Figs. 4(a,c)] is more robust with respect to  $\Gamma$  when compared to the orbital pumping [Figs. 4(b,d)]. This is because the relevant energy scale of the spin pumping is the exchange interaction, which is of the order of  $\sim 1$  eV. On the other hand, the SOC is necessary for the orbital pumping, whose energy scale is an order of magnitude smaller than the exchange interaction. This also explains a general tendency that Ni is more susceptible to  $\Gamma$  compared to Fe because the exchange interaction is significantly weaker in Ni than in Fe.

The experimental work by Hayashi *et al.* measured the DC component of the orbital pumping [25], which corresponds to

$\chi_{xx}^L w \sin^2 \theta_c$  in our theory. They found that the orbital pumping is significant in Ti/Ni while the effect is nearly absent in Ti/Fe, which seems consistent with our theoretical calculation. However, the numerical value of  $\chi_{xx}^L$  for Ni is approximately three times larger than that for Fe, which cannot explain almost complete suppression of the signal in Ti/Fe samples. Therefore, we conclude that the orbital pumping in the bulk ferromagnet alone cannot explain the experimental result. We speculate that the OAM transmission at the Ti/Fe interface could be much lower than that at the Ti/Ni interface.

Recent terahertz spectroscopy experiments have also revealed that ferromagnetic Ni can generate the OAM as it is excited by a pump laser [46–48]. Although the dynamics of magnetic moments is incoherent, which is different from the ferromagnetic resonance, we remark that the DC component projected onto the precession axis does not cancel as it is phase-independent (Fig. 1). Thus, our results imply that excitation of incoherent magnons by laser or temperature can induce OAM. In particular, we predict that when the gradient of such excitation is present, so-called *orbital Seebeck effect* can appear by a similar mechanism of the orbital pumping. Recently, El Hamdi *et al.* have shown that a temperature gradient can generate orbital currents, which is electrically measured via the inverse orbital Edelstein effect [49]. The experiment suggests that 6 percents of the OAM is injected compared to the spin for ferromagnetic Permalloy, which is in reasonable agreement with our calculation (Tab. I).

Meanwhile, in ferromagnets with low crystal symmetry, another mechanism that enables to induce the OAM from the thermal fluctuation of magnetic moments is via magnon-mediated chirality [50], which can result in an anomalous behavior of the  $g$ -factor as a function of the temperature [51]. Another way to generate the OAM by magnetization dynamics is to combine the spin pumping or the spin Seebeck effect with the spin-to-orbital conversion, which can be achieved by adding an insertion layer with strong SOC such as Pt. This idea was demonstrated in recent experiments [52, 53].

In conclusion, we have developed a theoretical formalism that describes the orbital pumping in ferromagnets. Unlike the spin pumping, the orbital pumping crucially depends on the SOC. We have performed first-principles calculations on ferromagnetic Fe, Co, and Ni for quantitative estimation of the magnitude. The results shows that the orbital pumping is strongest in Ni and weakest in Fe, whose magnitude ranges from 5 to 15 percents compared to the magnitude of the spin pumping. Our work opens the possibility of generating the OAM by magnetization dynamics and serves as a guideline for experiments.

D.G. acknowledges stimulating discussion with Michel Viret. We gratefully acknowledge the Jülich Supercomputing Centre for providing computational resources under project jiff40. This work was funded by the Deutsche Forschungsgemeinschaft (DFG, German Research Foundation) – TRR 173 – 268565370 (project A11), TRR 288 – 422213477 (project B06). K.A. acknowledges the support by JSPS KAKENHI (Grant Number: 22H04964, 20H00337, 20H02593), Spin-

tronics Research Network of Japan (Spin-RNJ), and MEXT Initiative to Establish Next-generation Novel Integrated Circuits Centers (X-NICS) (Grant Number: JPJ011438). A.P. acknowledges support from the ANR ORION project, grant ANR-20-CE30-0022-01 of the French Agence Nationale de la Recherche. A. M. acknowledges support from the Excellence Initiative of Aix-Marseille Université - A\*Midex, a French “Investissements d’Avenir” program.

---

\* [d.go@fz-juelich.de](mailto:d.go@fz-juelich.de)

- [1] J. Slonczewski, Current-driven excitation of magnetic multilayers, *Journal of Magnetism and Magnetic Materials* **159**, L1 (1996).
- [2] L. Berger, Emission of spin waves by a magnetic multilayer traversed by a current, *Physical Review B - Condensed Matter and Materials Physics* **54**, 9353 – 9358 (1996), cited by: 4202.
- [3] E. Myers, D. Ralph, J. Katine, R. Louie, and R. Buhrman, Current-induced switching of domains in magnetic multilayer devices, *Science* **285**, 867 – 870 (1999), cited by: 1212.
- [4] M. D. Stiles and A. Zangwill, Anatomy of spin-transfer torque, *Phys. Rev. B* **66**, 014407 (2002).
- [5] D. Ralph and M. Stiles, Spin transfer torques, *Journal of Magnetism and Magnetic Materials* **320**, 1190 (2008).
- [6] Y. Tserkovnyak, A. Brataas, and G. E. W. Bauer, Enhanced gilbert damping in thin ferromagnetic films, *Phys. Rev. Lett.* **88**, 117601 (2002).
- [7] Y. Tserkovnyak, A. Brataas, and G. E. W. Bauer, Spin pumping and magnetization dynamics in metallic multilayers, *Phys. Rev. B* **66**, 224403 (2002).
- [8] S. Mizukami, Y. Ando, and T. Miyazaki, Effect of spin diffusion on Gilbert damping for a very thin permalloy layer in Cu/permalloy/Cu/Pt films, *Phys. Rev. B* **66**, 104413 (2002).
- [9] A. Azevedo, L. H. Vilela Leão, R. L. Rodriguez-Suarez, A. B. Oliveira, and S. M. Rezende, dc effect in ferromagnetic resonance: Evidence of the spin-pumping effect?, *Journal of Applied Physics* **97**, 10C715 (2005).
- [10] E. Saitoh, M. Ueda, H. Miyajima, and G. Tatara, Conversion of spin current into charge current at room temperature: Inverse spin-Hall effect, *Applied Physics Letters* **88**, 182509 (2006).
- [11] Y. Tserkovnyak, A. Brataas, G. E. W. Bauer, and B. I. Halperin, Nonlocal magnetization dynamics in ferromagnetic heterostructures, *Rev. Mod. Phys.* **77**, 1375 (2005).
- [12] A. Brataas, Y. Tserkovnyak, G. E. W. Bauer, and P. J. Kelly, Spin pumping and spin transfer, in *Spin Current* (Oxford University Press, 2017).
- [13] P. M. Haney and M. D. Stiles, Current-Induced Torques in the Presence of Spin-Orbit Coupling, *Phys. Rev. Lett.* **105**, 126602 (2010).
- [14] D. Go, F. Freimuth, J.-P. Hanke, F. Xue, O. Gomonay, K.-J. Lee, S. Blügel, P. M. Haney, H.-W. Lee, and Y. Mokrousov, Theory of current-induced angular momentum transfer dynamics in spin-orbit coupled systems, *Phys. Rev. Res.* **2**, 033401 (2020).
- [15] D. Go and H.-W. Lee, Orbital torque: Torque generation by orbital current injection, *Phys. Rev. Research* **2**, 013177 (2020).
- [16] D. Lee, D. Go, H.-J. Park, W. Jeong, H.-W. Ko, D. Yun, D. Jo, S. Lee, G. Go, J. H. Oh, K.-J. Kim, B.-G. Park, B.-C. Min, H. C. Koo, H.-W. Lee, O. Lee, and K.-J. Lee, Orbital torque in magnetic bilayers, *Nature Communications* **12**, 6710 (2021).
- [17] S. Ding, A. Ross, D. Go, L. Baldrati, Z. Ren, F. Freimuth, S. Becker, F. Kammerbauer, J. Yang, G. Jakob, Y. Mokrousov, and M. Kläui, Harnessing Orbital-to-Spin Conversion of Interfacial Orbital Currents for Efficient Spin-Orbit Torques, *Phys. Rev. Lett.* **125**, 177201 (2020).
- [18] J. Kim, D. Go, H. Tsai, D. Jo, K. Kondou, H.-W. Lee, and Y. Otani, Nontrivial torque generation by orbital angular momentum injection in ferromagnetic-metal/Cu/Al<sub>2</sub>O<sub>3</sub> trilayers, *Phys. Rev. B* **103**, L020407 (2021).
- [19] S. Lee, M.-G. Kang, D. Go, D. Kim, J.-H. Kang, T. Lee, G.-H. Lee, J. Kang, N. J. Lee, Y. Mokrousov, S. Kim, K.-J. Kim, K.-J. Lee, and B.-G. Park, Efficient conversion of orbital Hall current to spin current for spin-orbit torque switching, *Communications Physics* **4**, 234 (2021).
- [20] G. Sala and P. Gambardella, Giant orbital Hall effect and orbital-to-spin conversion in 3d, 5d, and 4f metallic heterostructures, *Phys. Rev. Res.* **4**, 033037 (2022).
- [21] S. Dutta and A. A. Tulapurkar, Observation of nonlocal orbital transport and sign reversal of dampinglike torque in Nb/Ni and Ta/Ni bilayers, *Phys. Rev. B* **106**, 184406 (2022).
- [22] L. Liao, F. Xue, L. Han, J. Kim, R. Zhang, L. Li, J. Liu, X. Kou, C. Song, F. Pan, and Y. Otani, Efficient orbital torque in polycrystalline ferromagnetic-metal/Ru/Al<sub>2</sub>O<sub>3</sub> stacks: Theory and experiment, *Phys. Rev. B* **105**, 104434 (2022).
- [23] H. Hayashi, D. Jo, D. Go, T. Gao, S. Haku, Y. Mokrousov, H.-W. Lee, and K. Ando, Observation of long-range orbital transport and giant orbital torque, *Communications Physics* **6**, 32 (2023).
- [24] A. Bose, F. Kammerbauer, R. Gupta, D. Go, Y. Mokrousov, G. Jakob, and M. Kläui, Detection of long-range orbital-Hall torques, *Phys. Rev. B* **107**, 134423 (2023).
- [25] H. Hayashi and K. Ando, Observation of orbital pumping (2023), [arXiv:2304.05266 \[cond-mat.mes-hall\]](https://arxiv.org/abs/2304.05266).
- [26] L. Salemi and P. M. Oppeneer, First-principles theory of intrinsic spin and orbital Hall and Nernst effects in metallic monoatomic crystals, *Phys. Rev. Mater.* **6**, 095001 (2022).
- [27] Y.-G. Choi, D. Jo, K.-H. Ko, D. Go, K.-H. Kim, H. G. Park, C. Kim, B.-C. Min, G.-M. Choi, and H.-W. Lee, Observation of the orbital Hall effect in a light metal Ti, *Nature* **619**, 52 (2023).
- [28] F. Hund, Zur Deutung verwickelter Spektren, insbesondere der Elemente Scandium bis Nickel, *Zeitschrift für Physik* **33**, 345 (1925).
- [29] I. Levine, *Quantum Chemistry*, Pearson advanced chemistry series (Pearson, 2014).
- [30] D. Vanderbilt, *Berry Phases in Electronic Structure Theory: Electric Polarization, Orbital Magnetization and Topological Insulators* (Cambridge University Press, 2018).
- [31] See Supplemental Material, which also includes Refs. [30, 32–35, 54–57].
- [32] A. Bastin, C. Lewiner, O. Betbeder-matibet, and P. Nozieres, Quantum oscillations of the Hall effect of a fermion gas with random impurity scattering, *Journal of Physics and Chemistry of Solids* **32**, 1811 (1971).
- [33] L. Smrcka and P. Streda, Transport coefficients in strong magnetic fields, *Journal of Physics C: Solid State Physics* **10**, 2153 (1977).
- [34] A. Crépieux and P. Bruno, Theory of the anomalous hall effect from the kubo formula and the dirac equation, *Phys. Rev. B* **64**, 014416 (2001).
- [35] R. Kubo, A General Expression for the Conductivity Tensor, *Canadian Journal of Physics* **34**, 1274 (1956).
- [36] V. Bonbien and A. Manchon, Symmetrized decomposition of the Kubo-Bastin formula, *Phys. Rev. B* **102**, 085113 (2020).
- [37] E. Šimánek and B. Heinrich, Gilbert damping in magnetic mul-

- tilayers, *Phys. Rev. B* **67**, 144418 (2003).
- [38] D. L. Mills, Ferromagnetic resonance relaxation in ultrathin metal films: The role of the conduction electrons, *Phys. Rev. B* **68**, 014419 (2003).
- [39] B. A. Bernevig, T. L. Hughes, and S.-C. Zhang, Orbitronics: The Intrinsic Orbital Current in *p*-Doped Silicon, *Phys. Rev. Lett.* **95**, 066601 (2005).
- [40] H. Kontani, T. Tanaka, D. S. Hirashima, K. Yamada, and J. Inoue, Giant Orbital Hall Effect in Transition Metals: Origin of Large Spin and Anomalous Hall Effects, *Phys. Rev. Lett.* **102**, 016601 (2009).
- [41] D. Go, D. Jo, C. Kim, and H.-W. Lee, Intrinsic Spin and Orbital Hall Effects from Orbital Texture, *Phys. Rev. Lett.* **121**, 086602 (2018).
- [42] T. Yoda, T. Yokoyama, and S. Murakami, Orbital Edelstein Effect as a Condensed-Matter Analog of Solenoids, *Nano Letters* **18**, 916 (2018), pMID: 29373028.
- [43] L. Salemi, M. Berritta, A. K. Nandy, and P. M. Oppeneer, Orbitaly dominated Rashba-Edelstein effect in noncentrosymmetric antiferromagnets, *Nature Communications* **10**, 5381 (2019).
- [44] A. Johansson, B. Göbel, J. Henk, M. Bibes, and I. Mertig, Spin and orbital Edelstein effects in a two-dimensional electron gas: Theory and application to SrTiO<sub>3</sub> interfaces, *Phys. Rev. Res.* **3**, 013275 (2021).
- [45] F. Freimuth, S. Blügel, and Y. Mokrousov, Spin-orbit torques in Co/Pt(111) and Mn/W(001) magnetic bilayers from first principles, *Phys. Rev. B* **90**, 174423 (2014).
- [46] P. Wang, Z. Feng, Y. Yang, D. Zhang, Q. Liu, Z. Xu, Z. Jia, Y. Wu, G. Yu, X. Xu, and Y. Jiang, Inverse orbital Hall effect and orbitronic terahertz emission observed in the materials with weak spin-orbit coupling, *npj Quantum Materials* **8**, 28 (2023).
- [47] T. S. Seifert, D. Go, H. Hayashi, R. Rouzgar, F. Freimuth, K. Ando, Y. Mokrousov, and T. Kampfrath, Time-domain observation of ballistic orbital-angular-momentum currents with giant relaxation length in tungsten, *Nature Nanotechnology* [10.1038/s41565-023-01470-8](https://doi.org/10.1038/s41565-023-01470-8) (2023).
- [48] Y. Xu, F. Zhang, Y. Liu, R. Xu, Y. Jiang, H. Cheng, A. Fert, and W. Zhao, Inverse Orbital Hall Effect Discovered from Light-Induced Terahertz Emission (2023), [arXiv:2208.01866](https://arxiv.org/abs/2208.01866) [cond-mat.mes-hall].
- [49] A. El Hamdi, J.-Y. Chauleau, M. Boselli, C. Thibault, C. Gorini, A. Smogunov, C. Barreateau, S. Gariglio, J.-M. Triscone, and M. Viret, Observation of the orbital inverse Rashba-Edelstein effect, *Nature Physics* [10.1038/s41567-023-02121-4](https://doi.org/10.1038/s41567-023-02121-4) (2023).
- [50] L.-c. Zhang, D. Go, J.-P. Hanke, P. M. Buhl, S. Grytsiuk, S. Blügel, F. R. Lux, and Y. Mokrousov, Imprinting and driving electronic orbital magnetism using magnons, *Communications Physics* **3**, 227 (2020).
- [51] L. Alahmed, X. Zhang, J. Wen, Y. Xiong, Y. Li, L.-c. Zhang, F. Lux, F. Freimuth, M. Mahdi, Y. Mokrousov, V. Novosad, W.-K. Kwok, D. Yu, W. Zhang, Y. S. Lee, and P. Li, Evidence of Magnon-Mediated Orbital Magnetism in a Quasi-2D Topological Magnon Insulator, *Nano Letters* **22**, 5114 (2022), pMID: 35699946.
- [52] E. Santos, J. Abrão, D. Go, L. de Assis, Y. Mokrousov, J. Mendes, and A. Azevedo, Inverse Orbital Torque via Spin-Orbital Intertwined States, *Phys. Rev. Appl.* **19**, 014069 (2023).
- [53] R. Xu, H. Zhang, Y. Jiang, H. Cheng, Y. Xie, Y. Yao, D. Xiong, Z. Zhu, X. Ning, R. Chen, Y. Huang, S. Xu, J. Cai, Y. Xu, T. Liu, and W. Zhao, Giant orbit-to-charge conversion induced via the inverse orbital Hall effect (2023), [arXiv:2308.13144](https://arxiv.org/abs/2308.13144) [cond-mat.mtrl-sci].
- [54] D. Wortmann, G. Michalicek, N. Baadji, M. Betzinger, G. Bihlmayer, J. Bröder, T. Burnus, J. Enkovaara, F. Freimuth, C. Friedrich, C.-R. Gerhorst, S. Granberg Cauchi, U. Grytsiuk, A. Hanke, J.-P. Hanke, M. Heide, S. Heinze, R. Hilgers, H. Janssen, D. A. Klüppelberg, R. Kovacik, P. Kurz, M. Lezaic, G. K. H. Madsen, Y. Mokrousov, A. Neukirchen, M. Redies, S. Rost, M. Schlipf, A. Schindlmayr, M. Winkelmann, and S. Blügel, *FLEUR*, Zenodo (2023).
- [55] J. P. Perdew, K. Burke, and M. Ernzerhof, Generalized Gradient Approximation Made Simple, *Phys. Rev. Lett.* **77**, 3865 (1996).
- [56] E. Wimmer, H. Krakauer, M. Weinert, and A. J. Freeman, Full-potential self-consistent linearized-augmented-plane-wave method for calculating the electronic structure of molecules and surfaces: O<sub>2</sub> molecule, *Phys. Rev. B* **24**, 864 (1981).
- [57] G. Pizzi, V. Vitale, R. Arita, S. Blügel, F. Freimuth, G. Géranton, M. Gibertini, D. Gresch, C. Johnson, T. Koretsune, J. Ibañez-Azpiroz, H. Lee, J.-M. Lihm, D. Marchand, A. Marrazzo, Y. Mokrousov, J. I. Mustafa, Y. Nohara, Y. Nomura, L. Paulatto, S. Poncé, T. Ponweiser, J. Qiao, F. Thöle, S. S. Tsirkin, M. Wierzbowska, N. Marzari, D. Vanderbilt, I. Souza, A. A. Mostofi, and J. R. Yates, Wannier90 as a community code: new features and applications, *Journal of Physics: Condensed Matter* **32**, 165902 (2020).